Flat band and Lifshitz transition in long-range-ordered supergraphene obtained by Erbium intercalation

Ahmad Zaarour, Vincent Malesys, Joan Teyssandier, Marion Cranney, Emmanuel Denys, Jean-Luc Bubendorff, Alban Florentin, Ludovic Josien, François Vonau, Dominique Aubel, et al.

Flat band and Lifshitz transition in long-range-ordered supergraphene obtained by Erbium intercalation

A. Zaarour,[1] V. Malesys,[1] J. Teyssandier,[1] M. Cranney,[1] E. Denys,[1] J. L. Bubendorff,[1] A. Florentin,[1] L. Josien,[1] F. Vonau,[1] D. Aubel,[1] A. Ouerghi,[2] C. Bena,[3] and L. Simon[1,*]

[1]*Université de Haute-Alsace, CNRS, Institut de Science des Matériaux de Mulhouse UMR 7361, 3Bis rue Alfred Werner, 68093 Mulhouse, France and Université de Strasbourg (UniStra), F-67081 Strasbourg, France*

[2]*Université Paris-Saclay, CNRS, Centre de Nanosciences et de Nanotechnologies, 91120 Palaiseau, France*

[3]*Institut de Physique Théorique, Université Paris Saclay, CEA CNRS, Orme des Merisiers, 91190 Gif-sur-Yvette Cedex, France*

(Received 9 September 2022; revised 7 November 2022; accepted 14 December 2022; published 13 February 2023)

We report the observation of graphene doped up to the Lifshitz transition obtained solely by the intercalation of Erbium atoms. ARPES measurements show that a wide flat band is generated around the *M* point of the Brillouin zone. We propose that this is the effect of an induced spin-orbit coupling. Scanning Tunneling Microscopy (STM) experiments reveal a longrange ordered hexagonal superstructure: we argue that this reflects the ordering of the intercalated Er atoms acting as impurities. This system provides a playground to study the interaction between a magnetic order and a divergent density of states at the Fermi level.

DOI: 10.1103/PhysRevResearch.5.013099

I. INTRODUCTION

A flat band is a nondispersive region in the electronic band structure of a material, for which a high electron density and increased electronic interactions are expected. With the recent discovery of the superconductivity in twisted bilayer graphene at the magic angle, and in rhombohedral graphene, all involving flat bands [1–3], as well as with the observation of flat bands in some high-Tc cuprate superconductors [4–7], the possibility to reach the flat bands around the *M* points in graphene is of high importance for many possible applications to realize nonconventional high-Tc superconductivity in the so-called van Hove scenario [8]. Thus, it became very interesting to explore the possibility to reach extremely high levels of electron doping corresponding to these critical points of its Brillouin zone.

Among the proposed approaches, the intercalation of metallic atoms was considered as an efficient way to engineer the graphene electronic band structure and obtain high doping levels. Earlier observations were obtained with noble metals such as gold [9–13] and strongly inspired by the historical results observed in graphite intercalation compounds, and motivated by the possible observation of superconductivity for such system, other atoms such as Li, K, Ca, Cs, and Rb [14] have also been considered. Most of these studies are done using the well-oriented epitaxial graphene on SiC(0001) (allowing band structure measurements), which consists in a buffer layer (BuL) graphene partially covalently bonded to the SiC substrate, and one or more graphene layers in van der Waals interaction with the BuL. As it was first shown for hydrogen intercalation [15], by breaking the covalent bonds with the substrate, the BuL itself can be transformed in a decoupled quasi-free-standing graphene monolayer (QFSMLG).

A van Hove singularity extension was observed with combined Ca intercalation under and deposition on top of epitaxied graphene on SiC [16], and Lifshitz transition has also been reported in the case of overdoping G/Ir(111) by Cs deposition [17]. It appears that the lanthanide atoms are among the most reactive, reaching electron densities one order of magnitude higher than for other elements such as alkali metals [18]. The highest value of *n* doping observed so far has been obtained more recently [19] through a combination of Yb intercalation and a subsequent K adsorption on top reaching the Lifshitz transition. The Fermi surface in this case shows a flat band around the *M* point, extending in the direction $\overline{KMK'}$ when doping by Yb intercalation, and becoming less and less elongated beyond the Lifshitz transition in the presence of K adsorption. More recently, by using the intercalation of Li atoms on G-ML on SiC(0001), a doubling of the Dirac cone has been observed, with the highly *n* doped one corresponding to an electron density of 5.6×10^{14} cm^{-2} [20]. In spite of this high electron density, the Lifshitz transition has not been reached. A so called van Hove singularity extension has been noted, with small flat band segments observed along the line connecting the apex of the two trigonal constant energy contours in the direction $\overline{KMK'}$.

In the present study, following this line of thought, we wanted to explore the properties of graphene in the presence of intercalated Er atoms. These atoms allow us to also study the interplay between the atomic magnetic moments and graphene, and possibly induce some spin-orbit coupling. Our goal was to obtain a highly *n*-doped QFSMLG by the

*Corresponding author: Laurent.simon@uha.fr

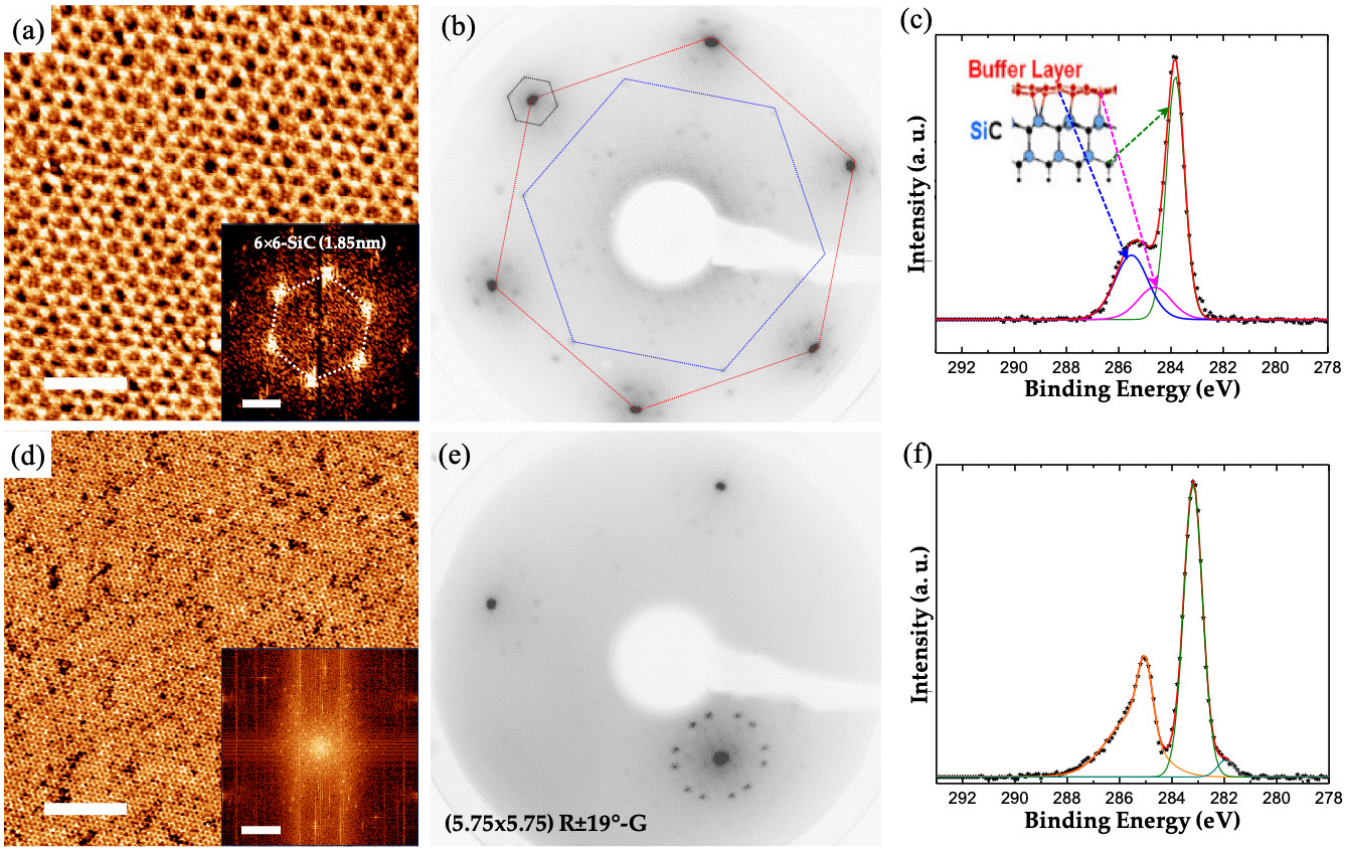

FIG. 1. (a) STM image of the pristine BuL layer; $40 \times 40\,\text{nm}^2$, $V_S = -1.67\,\text{V}$, $I = 500\,\text{pA}$, $Scale = 8\,\text{nm}$. The inset in (a) shows the Fourier Transform (FT) (Scale $3\,\text{nm}^{-1}$) of the topographic image with the 6×6-SiC reconstruction (black hexagon) which is found also in the LEED pattern in (b). The red and blue hexagon correspond to the G-1×1 and SiC-1×1 respectively. (c) XPS C1s core level peak measured with a monochromatized Al_{K_α} source showing typical components attributed to the atoms indicated in the inset scheme. (d) STM topographic image after the ordered Er intercalation; $-1.63\,\text{V}; 500\,\text{pA}; 120 \times 120\,\text{nm}^2$, Scale $= 25\,\text{nm}$ with the FT of the topographic image in the inset indicating a monodomain (Scale $17\,\text{nm}^{-1}$). In (e) the typical LEED pattern around the specular spot shows a $(5.75 \times 5.75)R19^\circ$ pattern with two domain orientations. (f) shows the typical C1s core level peak after Er intercalation, with the disappearance of the components associated with BuL in favor of the component associated with a ML (image processing using the WSxM software [21]).

decoupling of the BuL, to reach the Lifshitz transition and to recover an ordered intercalation.

II. EXPERIMENTAL DETAILS

We started with a well developed $(6\sqrt{3} \times 6\sqrt{3})R30^\circ$ pattern starting from the SiC(0001) substrate. Figure 1(a) shows a large area of buffer layer. The characteristic LEED pattern in (b) shows the well-known 6×6-SiC reconstruction relative to the 1×1 Bravais lattice of the topmost silicon atoms of the SiC (0001) substrate. The C1s core level peak characteristic to a pure buffer layer is shown in (c). This core level peak is decomposed in three components, one corresponding to the carbon in the SiC substrate, one associated to the C-C bonds in the BuL, and one with the covalent bond between the C atoms in the BuL and the silicon of the substrate.

The intercalation is performed by the deposition of 1 ML of Erbium atoms following by annealing at $1000\,^\circ\text{C}$ during several hours at vacuum down to $1 - 2.10^{-11}$ mbar. During the annealing the LEED should be checked regularly (each hour) to avoid the desorption of Er atoms after the complete development of the phase.

III. RESULTS AND DISCUSSION

The STM image shows large terraces, and the whole sample gives the characteristic LEED pattern in (e), for which we show here the central specular spot. We observe a hexagonal structure giving two spots at a $\pm 19^\circ$ angle with respect to the (1×1) graphene lattice. These spots correspond to two domains that can be observed on the same terrace. Here the large terrace in (d) corresponds to a mono domain. In the core level peak C1s depicted in (f) we note the component corresponding to the carbon in SiC, the disappearance of the two BuL components, and the formation of a peak attributed to the QFSMLG. Usually, for a pristine ML graphene this component is much more symmetrical. Here it is necessary to add a supplementary component in the fitting procedure to capture the peak tailing, characteristic of metallic systems but with a much higher asymmetry. Such asymmetry has been attributed to a high level of electron doping [22].

Subsequently, in order to study the band structure of this system, we have performed Angle Resolved Photoemission-Spectroscopy (ARPES) measurements. Figures 2(a)–2(c) show, respectively, the dispersion curves around the K and M points, and the Fermi surface. The inset schematics show the

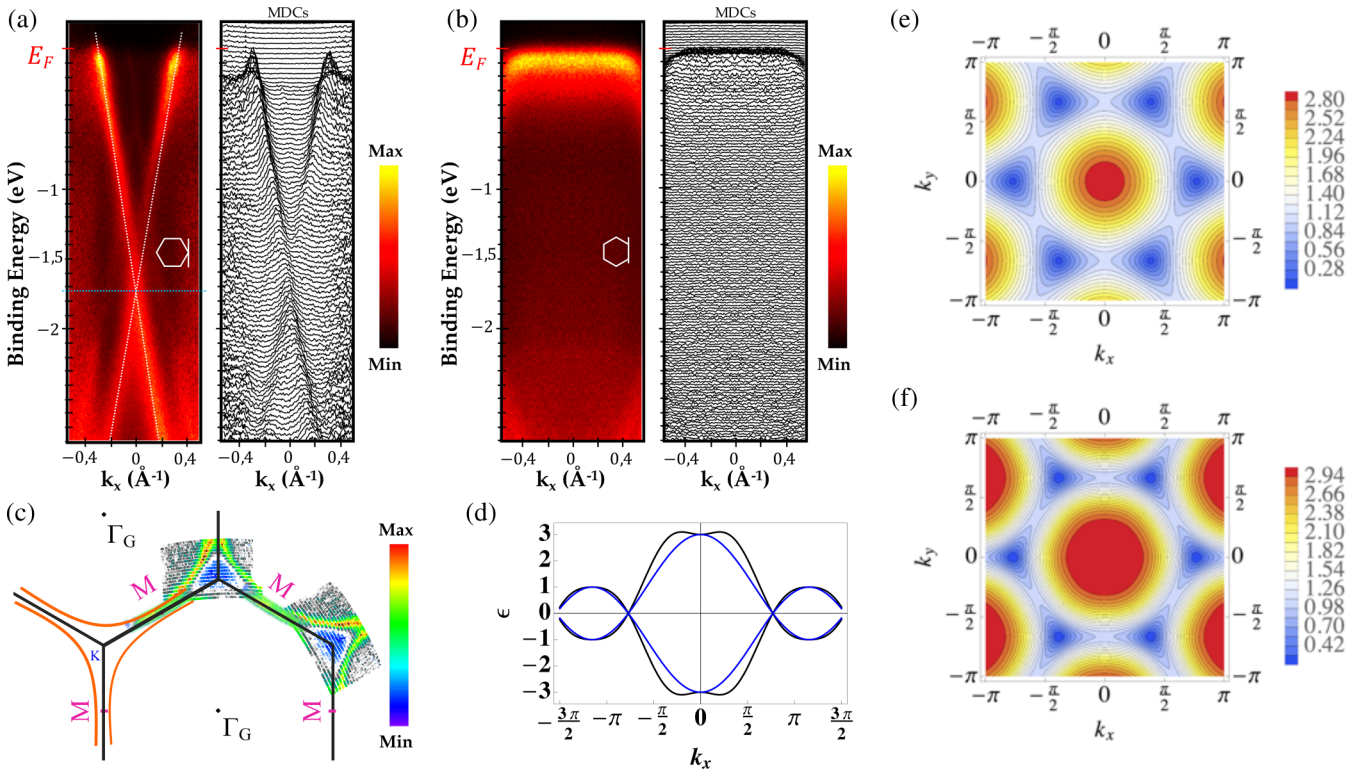

FIG. 2. ARPES measurements using an electron analyser Scienta-R3000 and a nonmonochromatized UV sourve $h\nu = 40.8$ eV. The dispersion curves measured along the directions indicated in the insets, are given with the corresponding MDC around the K point in (a) and around the M point in (b). The Fermi surface is reconstructed and shown in (c). (d) An energy dispersion cut at $k_y = 0$ for pristine graphene with no spin-orbit coupling (SOC) (blue), and with an induced PIA of SOC of 0.8 (black), measured in units of the bandwidth (3.3 eV). (e) and (f) Equal energy contours for graphene with no SOC in (e) and a 0.8 PIA SOC in (f).

investigated paths in momentum space. Thus, in Fig. 2(a), in the vicinity of the K point we can see a Dirac cone with a perfect linear dispersion, and with a Dirac point at -1.72 eV under the Fermi level, without any gap opening or other modification of the dispersion. As opposed to what we have previously observed for Tb intercalation [18] and in spite of the large n doping, the dispersion remains linear up to the Fermi level, with no significant kink usually attributed to electron-phonon coupling. Around the point M, as depicted in Fig. 2(b), we observe a flat band, up to 0.91 Å^{-1} wide. The kink near the Fermi level is much more visible at the edge of the flat band than around the K point.

Based on these observations we deduce that the only possible Fermi surface contour is the orange line drawn in Fig. 2(c). This has been cross-checked with a direct measure of the Fermi surface obtained by fixing the energy and varying the photon incidence angle. We clearly see a triangular contour around the K point and the continuous flat band crossing the van Hove singularity at the M point. We deduce that the Lifshitz transition is reached. The density of electrons calculated using the Luttinger theorem [23] (corresponding to the filling of the region between the FS inner contour and the hexagon defining the first Brillouin zone) is 5.1×10^{14} cm^{-2}, which is one of the highest electron doping ever contained solely by intercalation, without any dopant deposited on top of graphene, as it was done with K in for Yb intercalation [19]. We think that this level of doping can be more easily reached with Erbium than Yb as the hybridization between the 4f states and the π graphene band states can be ruled out since the Er 4f states are at a higher binding energy (3 eV for Yb and 9 eV for Er) [24]. We also notice that, in contrast to what has been pointed out recently for Li-intercalated graphene on Cobalt [25], we do not observe a gap opening; this is a supplementary argument ruling out a possible effect of the hybridization on the Fermi surface shape at the Lifshitz transition.

We investigate first if these band structure modifications may be connected to the formation of covalent bonds between Si and Erbium. As both Si2p core level peaks measured by XPS are unchanged before and after Erbium intercalation we argue that this is not the case. In the same way, the Er4d spectrum measured after intercalation is strongly similar with the spectrum recorded on a 2.5 nm thick Erbium layer [Supplemental Material (SM) [26]]. The metallic character of the atoms is thus preserved. We subsequently turn toward an explanation based on the magnetic nature of the Er atoms and the possibility to induce a nonzero SOC in the monolayer graphene. This has been discussed, for example, in [27]. Various SOC terms are discussed, including the Rashba SOC and the intrinsic Kane-Mele-like one. However, we are looking here for a SOC mediated by the π states in graphene, which preserves the band structure features that we observe, particularly no gap opening and a flattening of the Fermi surface along the direction $\overline{KMK'}$. It turns out that the only

SOC term that can satisfy these constraints is the spinflipping next nearest neighbor SOC, denoted principal-plane mirror asymmetry induced SOC, or PIA [27].

We have performed tight-bind calculations using such an effective SOC term with various possible values of the induced SOC. In Fig. 2(d) we plot the energy dispersion obtained from diagonalizing the TB Hamiltonian in [27], the blue curve corresponds to the pristine graphene, and the black curve to a PIA SOC with a value of 0.8 (in units of the graphene bandwidth, 3.3 eV), while Figs. 2(e) and 2(f) show the equal energy contours for these two cases. The calculations indeed show a linear dispersion at the K point, an increase of the Fermi velocity along the direction $\overline{\Gamma KM}$, no gap opening at the Dirac points, and a flattening of the band around the M point. This exemplarily demonstrates that for a PIA SOC coupling of 0.8 the main characteristic of the ARPES measured band structure are reproduced, for example, the fact that the Fermi surface is elongated along $\overline{KMK'}$, the same as the one measured by ARPES [see Fig. 2(c)]. This supports our hypothesis that the effect of the Er intercalation is to induce a large effective SO PIA coupling term in the QFSMLG.

Let us now move to investigate the nature of this new phase as observed by STM measurements. In Fig. 3(a) we show the 3D representation of a well-ordered region of the surface exhibiting the supergraphene phase. This 3D representation allows one to show the QFSMLG which is fully continuous over the large hexagons. We see a higher intensity and some sort of electron delocalization along the edges of each large hexagon. As this is observed for different directions in the same image this is definitively not a tip artefact. In Fig. 3(b) we depict a larger area with some defects in black, corresponding probably to missing intercalated atoms (see as well [26]), as the top graphene layer is continuous over the entire area. This new structure is difficult to explain, particularly the angle of $\pm 19^\circ$ between the superstructure and the graphene lattice. This phase strongly looks like a Moiré pattern, and as argued in SM [26], it may correspond to two superposed identical graphene layers rotated by 10°. However, as proven by the ARPES measurements, we have only one graphene layer. We have also tested other Moiré patterns, between the top graphene layer and an intercalated monolayer of Erbium, with or without the SiC(0001) underneath, with different lattice vectors for the Erbium ML, and different rotation angles between the atomic planes, but all these hypotheses have failed to explain the observed structure [26].

An accurate examination of this phase shows that the top graphene layer is perturbed along its lattice direction [see the blue arrows in Fig. 3(a)]. Thus, the only possibility to explain the observed ordered phase [defined by the lattice vector in yellow in Fig. 3(a)] and its disorientation with the graphene lattice is to consider that we have Erbium intercalated atoms at the apex of a honeycomb structure with two atoms per unit cell and a lattice constant of 1.42 nm, as schematized in Fig. 3(e). This first proposed simple model predicts the correct angle of 19° with the original graphene lattice. We have found that this structure corresponds to a commensuration of Erbium atoms (in red) with the T_4 site of the topmost 1×1 silicon atoms (in blue) of the SiC substrate [see the dotted circle in Fig. 3(e)]. This is the only commensuration that we have noted.

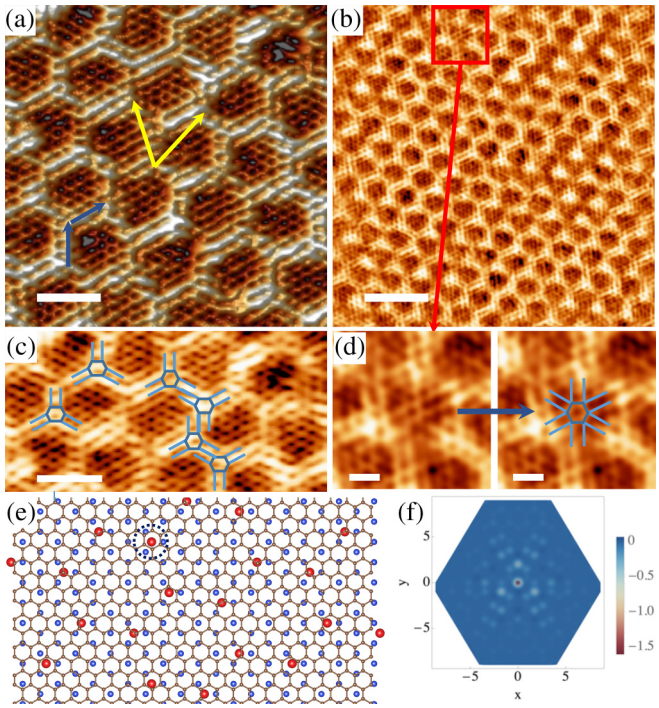

FIG. 3. (a) 3D representation of topographic STM image $6 \times 6\,\text{nm}^2$; V $= -20$ mV; I $= 500$ pA, Scale $= 1.2$ nm. Blue arrows show the direction of the graphene lattice, and the yellow arrows indicate the unit cell of the $(5.75 \times 5.75)R19^\circ$ superstructure. (b)15×15 nm^2 Scale $= 2.9$ nm; V $= -207$ mV; I $= 500$ pA with zoom-ins in (c) (Scale $= 1.2$ nm) and (d). In (d) (Scale $= 0.5$ nm) a zoom-in of the area in the red square shows a single impurity in the middle of a large hexagon with a six-fold symmetry in the LDOS. (e) shows a possible model with a honeycomb organization of the intercalated Er atoms which act as impurities. The carbon atoms of the top graphene layer are denoted in black, the Er atoms in red, and the silicon atoms of the substrate in blue. The black dotted circle surrounding an Er atom at the T_4 site highlights the commensuration of the phase with the substrate. (f) Modification of the LDOS in graphene induced at the Lifshitz transition by an impurity, for a SO PIA coupling of 0.8.

From XPS measurements we estimated at 2.8% the ratio of Er atoms to the C atoms in the graphene layer [28]. With this first model we have 3% of Erbium and considering that we can have up to 3 electrons per each Er atom (Er^{3+}), the expected electron density is $3.5 \times 10^{14}\,\text{cm}^{-2}$ which is lower but comparable with the density evaluated from ARPES. We notice that the precision of our Fermi surface measurement is quite low due to the thickness of our analyser slit.

Given the above arguments, we claim that the observed graphene superstructure is rather explained by the intercalated Erbium atoms acting as impurities which modify the local density of states of the graphene monolayer (LDOS). We base our argument on analyzing first an isolated defect in graphene [see Figs. 3(b) and 3(d)], which is not a part of the ordered Er superstructure. For such a defect we observe a small hexagon in the center, which corresponds to an aromatic carbon ring. The LDOS seems to extend into a six-fold star-like structure

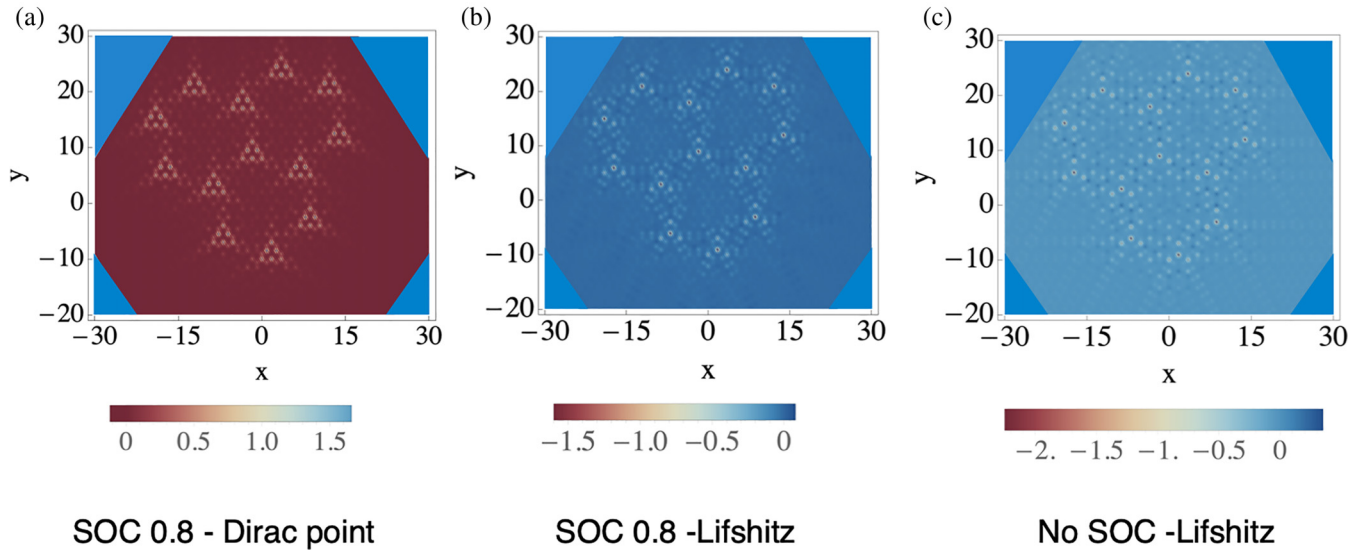

FIG. 4. Modifications induced by a network of impurities to the LDOS of graphene: (a) at the Dirac-point energy with a PIA spin-orbit coupling of 0.8, (b) at the Lifshitz transition with a PIA spin-orbit coupling of 0.8, and (c) at the Lifshitz transition with no-spin orbit coupling. We take the impurity potential to be equal to 100 times the bandwidth but the results depend very little qualitatively on the chosen value of the impurity potential.

with six wings originating on the six edges of the aromatic ring. We depict a schematic of this six-fold (6C) symmetry structure by the blue lines in Fig. 3(d). We compare this to a real-space T-matrix formalism [29] of the impurity-induced LDOS in the vicinity of a localized impurity in graphene at the Lifshitz transition, in the presence of the effective spin-orbit coupling (SOC PIA of 0.8) that we have proposed to explain the observed characteristics of the band structure measured by ARPES. The resulting LDOS is depicted in Fig. 3(f). We see that indeed the theoretical calculation reproduces reasonably well the observed impurity feature.

When the Er impurities are ordered into a honeycomb structure it appears that the LDOS in the vicinity of each impurity exhibits rather an effective three-fold (3C) symmetry [see Fig. 3(c)]. The difference between the network 3C symmetry and single impurity 6C symmetries is discussed in what follows. By schematizing the impurities as small hexagons and a star-like feature made of three sets of double lines originating on three sides of the hexagon, symbolizing the extension of the LDOS modifications, we see that it is possible to generate the supergraphene phase. The angle of $\pm 19^\circ$ is thus a result of the position of the Er impurities which also gives rise to a register shift between the pair of lines which schematize the delocalization of charge. This simple picture is supported by a detailed theoretical analysis. In Figs. 4(a)–4(c), using the T-matrix formalism, we show LDOS calculations for a number of impurities placed at the positions expected for the Er atoms in the hexagonal superstructure. For comparison we evaluate the LDOS for an effective PIA SOC of 0.8 at the Dirac point (a), and at the Lifshitz transition (b), as well as for a pristine graphene layer at the Lifshitz transition (c). While we observe a "standard" $(\sqrt{3} \times \sqrt{3})R30^\circ$ reconstruction around the defect at the Dirac point, we note that at the Lifshitz transition each impurity gives rise rather to a LDOS pattern with a six-fold symmetry, similar to the STM patterns observed in Fig. 3. When ordering the Er impurities into a honeycomb lattice slightly rotated with respect to the graphene one, the effect is to enhance the visibility of the LDOS modifications along the three lines connecting one Er atom to its neighbors and thus give rise to an apparent 3C symmetry rather than to a 6C one as it is the case for an isolated impurity. Moreover, the induced PIA SOC also enhances the interference effect and the intensity of the standing wave along the direction which links the two impurities. This allows us to obtain a good agreement with the observed $(5.75 \times 5.75)R19^\circ$ phase.

There is another effect that may contribute to these observations that cannot be taken into account by our coupled TB and T-matrix calculation: it is highly likely that the observed supergraphene phase is also characterized by a Kekulé distortion (KD) which modifies even more deeply the LDOS patterns, and in particular may contribute to the reinforcement of the density of state between the intercalated Er atoms. Such KD order has been observed for undoped graphene on Ag(111) surfaces: here the Fermi level lies at the Dirac point, and the resulting LDOS impurity patterns will give rise to a $\sqrt{3} \times \sqrt{3}R30^\circ$ reconstruction. When the distance and the orientation between the impurities is in commensuration with the standing wave pattern, the electron-lattice interaction gives rise to atomic displacements of the carbon atoms and to the development of the Kekulé distortion phase [30]. For our system the Fermi level is at the Lifshitz transition and the QPI patterns are characterized by the structure described in Fig. 3(d). Assuming that a KD associated with these patterns arises, we expect that some of the effects observed in the impurity-perturbed LDOS to be enhanced, as well as to be generalized at all energies: when a strong order appears because of the KD, the standing wave patterns are rather charge density waves (CDW) than Friedel oscillations (CDW differ from Friedel oscillation by the fact that there is no dispersion with energy). Indeed, we have measured the Fourier Transform of the dI/dV map images and found that the maps

are energy independent [Supplemental Material (SM) [26]]. Nevertheless, the STM image (in direct space) shows that the intensity of the edges of the hexagon is high at the Fermi level and decreases for higher energies. However, a more detailed experimental and theoretical analysis would be necessary to argue definitely in the favor of the existence of a Kekulé distortion phase. Our results thus provide a starting point to investigate the LDOS impurity patterns, as well as the existence of a possible KD in graphene when the Fermi level lies at the Lifshitz transition.

IV. CONCLUSION

In conclusion we report here an ordered, highly n-doped, free-standing supergraphene phase obtained by the intercalation of Erbium atoms. The intercalated Erbium atoms seem to lie free inbetween the top graphene layer and the SiC substrate, forming no bond with the silicon atoms. The observed hexagonal superstructure is in good agreement to impurity-induced features generated by the ordered Er atom network, and raises questions about the existence of a Kekulé distortion phase. The band structure measured by ARPES reveals a robust linear dispersion with a Dirac point at an energy of -1.72 eV under the Fermi level, and no gap opening. The measurement of the Fermi surface indicates that the Lifshitz transition has been reached with an electron density reaching $5.1 \pm 0.8 \times 10^{14}$ cm^2 and reveals a flattening of the band around the M point. Using tight-binding calculations we have studied the possibility to induce an effective SOC in graphene in this configuration, that can explain in particular the modifications of the band structure and the flattening of the Fermi contour around the *M* points. While the type of SOC chosen does not open a gap and respects the linearity of the dispersion almost up to the Fermi level (in agreement with the ARPES observations), the energy of the SOC used in the calculations (2.6 eV) is very high and can even be considered unrealistic. We are thus aware that the model proposed here may not be the only explanation for the observed features, however at present a more comprehensive theoretical review of other alternatives, and especially a thorough experimental analysis, are needed to distinguish between different possible scenarios. This is beyond the scope of this work, which provides however substantial insight to motivate further experiments and theoretical investigations of this problem.

ACKNOWLEDGMENTS

This work has benefited from a government grant managed by the National Research Agency (ANR) under the program "Investissements d'avenir"-Mat-Light 4.0 (Grant No. ANR-21-EXES-0012) and the project MIXES (Grant No. ANR-19-CE09-0028). It is also supported by the Région Grand Est and European fond Feder through the "NanoteraHertz" Project.

[1] Y. Cao, V. Fatemi, A. Demir, S. Fhang, S. L. Tomarken, J. Y. Luo, J. D. Sanchez-Yamagishi, K. Watanabe, T. Taniguchi, E. Kaxiras, R. C. Ashoori, and P. Jarillo-Herrero, Correlated insulator behaviour at half-filling in magic-angle graphene superlattices, Nature (London) **556**, 80 (2018).

[2] H. Zhou, T. Xie, T. Taniguchi, K. Watanabe, and A. F. Young, Superconductivity in rhombohedral trilayer graphene, Nature (London) **598**, 434 (2021).

[3] Y. Cao, V. Fatemi, S. Fhang, K. Watanabe, T. Taniguchi, E. Kaxiras, and P. Jarillo-Herrero, Unconventional superconductivity in magic-angle graphene superlattices, Nature (London) **556**, 43 (2018).

[4] K. Gofron, J. C. Campuzano, A. A. Abrikosov, M. Lindroos, A. Bansil, H. Ding, D. Koelling, and B. Dabrowski, Observation of an "Extended" Van Hove Singularity in $YB_{a_2}Cu_4O_8$ by Ultrahigh Energy Resolution Angle-Resolved Photoemission, Phys. Rev. Lett. **73**, 3302 (1994).

[5] D. H. Lu, M. Schmidt, T. R. Cummins, S. Schuppler, F. Lichtenberg, and J. G. Bednorz, Fermi Surface and Extended van Hove Singularity in the Noncuprate Superconductor Sr_2RuO_4, Phys. Rev. Lett. **76**, 4845 (1996).

[6] I. I. Mazin, Intercalant-Driven Superconductivity in YbC_6 and CaC_6, Phys. Rev. Lett. **95**, 227001 (2005).

[7] V. Yu. Irkhin, A. A. Katanin, and M. I. Katsnelson, Robustness of the Van Hove Scenario for High-T_c Superconductors, Phys. Rev. Lett. **89**, 076401 (2002).

[8] R. Nandkishore, L. S. Levitov, A. V. Chubukov, Chiral superconductivity from repulsive interactions in doped graphene, Nat. Phys. **8**, 158 (2012).

[9] B. Premlal, M. Cranney, F. Vonau, D. Aubel, D. Casterman, M. M. De Souza, and L. Simon, Surface intercalation of gold underneath a graphene monolayer on SiC(0001) studied by scanning tunneling microscopy and spectroscopy, Appl. Phys. Lett. **94**, 263115 (2009).

[10] M. Cranney, F. Vonau, P. B. Pillai, E. Denys, D. Aubel, M. M. De Souza, C. Bena, and L. Simon, Superlattice of resonators on monolayer graphene created by intercalated gold nanoclusters, Europhys. Lett. **91**, 66004 (2010).

[11] M. N. Nair, M. Cranney, F. Vonau, D. Aubel, P. Le Fèvre, A. Tejeda, F. Bertran, A. Taleb-Ibrahimi, and L. Simon, High van Hove singularity extension and Fermi velocity increase in epitaxial graphene functionalized by intercalated gold clusters, Phys. Rev. B **85**, 245421 (2012).

[12] M. N. Nair, M. Cranney, T. Jiang, S. Hajjar-Garreau, D. Aubel, F. Vonau, A. Florentin, E. Denys, M.-L. Bocquet, and L. Simon, Noble-metal intercalation process leading to a protected adatom in a graphene hollow site, Phys. Rev. B **94**, 075427 (2016).

[13] S. Forti, S. Link, A. Stöhr, Y. Niu, A. A. Zakharov, C. Coletti, and U. Starke, Semiconductor to metal transition in two-dimensional gold and its van der Waals heterostack with graphene, Nat. Commun. **11**, 2236 (2020).

[14] L. Daukiya, M. N. Nair, M. Cranney, F. Vonau, S. Hajjar-Garreau, D. Aubel, and L. Simon, Functionalization of 2D materials by intercalation, Prog. Surf. Sci. **94**, 1 (2019).

[15] C. Riedl, C. Coletti, T. Iwasaki, A. A. Zakharov, and U. Starke, Quasi-Free-Standing Epitaxial Graphene on SiC Obtained by Hydrogen Intercalation, Phys. Rev. Lett. **103**, 246804 (2009).

[16] J. L. McChesney, A. Bostwick, T. Ohta, T. Seyller, K. Horn, J. González, and E. Rotenberg, Extended van Hove Singularity

and Superconducting Instability in Doped Graphene, Phys. Rev. Lett. **104**, 136803 (2010).

[17] M. G. Hell, N. Ehlen, B. V. Senkovskiy, E. H. Hasdeo, A. Fedorov, D. Dombrowski, C. Busse, T. Michely, G. di Santo, L. Petaccia, R. Saito, and A. Grüneis, Resonance Raman Spectrum of Doped Epitaxial Graphene at the Lifshitz Transition, Nano Lett. **18**, 6045 (2018).

[18] L. Daukiya, M. N. Nair, S. Hajjar-Garreau, F. Vonau, D. Aubel, J. L. Bubendorff, M. Cranney, E. Denys, A. Florentin, G. Reiter, and L. Simon, Highly n-doped graphene generated through intercalated terbium atoms, Phys. Rev. B **97**, 035309 (2018).

[19] P. Rosenzweig, H. Karakachian, D. Marchenko, K. Küster, and U. Starke, Overdoping Graphene beyond the van Hove Singularity, Phys. Rev. Lett. **125**, 176403 (2020).

[20] C. Bao, H. Zhang, X. Wu, S. Zhou, Q. Li, P. Yu, J. Li, W. Duan, and S. Zhou, Coexistence of extended flat band and Kekulé order in Li-intercalated graphene, Phys. Rev. B **105**, L161106 (2022).

[21] I. Horcas, R. Fernández, J. M. Gómez-Rodríguez, J. Colchero, J. Gómez-Herrero, A. M. Baro, WSXM: A software for scanning probe microscopy and a tool for nanotechnology, Rev. Sci. Instrum. **78**, 013705 (2007).

[22] B. E. Sernelius, Core-level spectra from graphene, Phys. Rev. B **91**, 045402 (2015).

[23] J. M. Luttinger, Fermi surface and some simple equilibrium properties of a system of interacting Fermion, Phys. Rev. **119**, 1153 (1960).

[24] J. F. Moulder and J. Chastain, Handbook of x-ray photoelectron spectroscopy: A reference book of standard spectra for identification and interpretation of XPS data. Eden Prairie, Minn: Physical Electronics Division, Perkin-Elmer Corp (1992).

[25] M. Jugovac, C. Tresca, I. Cojocariu, G. Di Santo, W. Zhao, L. Petaccia, P. Moras, G. Profeta, and F. Bisti, Clarifying the apparent flattening of the graphene band near the van Hove singularity, Phys. Rev. B **105**, L241107 (2022).

[26] See Supplemental Material at http://link.aps.org/supplemental/10.1103/PhysRevResearch.5.013099 for the reproduction of the supergraphene phase as a Moiré pattern obtained by the superposition of two layers of graphene rotated by 10° (Fig. 1). XPS Si2p and Er4d core level peaks (Fig. 2). An STM analysis of point defects observed in the supergraphene structure (Fig. 3). Simulation of Moiré patterns obtained by the stacking of the SiC(0001) substrate below one rotated Er monolayer with a graphene plane on top (Fig. 4). dI/dV STM images and Fourier transforms obtained at different bias voltages (Fig. 5).

[27] D. Kochan, S. Irmer, and J. Fabian, Model spin-orbit coupling Hamiltonians for graphene systems, Phys. Rev. B **95**, 165415 (2017).

[28] The Er content is calculated with the ratio of the $4d_{3/2}$ core level component of Er 4d by the area of the C1s-G component of the C1s core level component. A RSF of 12.6 is considered giving 5.04 for the $4d_{3/2}$ component.

[29] L. Simon, C. Bena, F. Vonau, M. Cranney, and D. Aubel, Fourier-transform scanning tunnelling spectroscopy: the possibility to obtain constant-energy maps and band dispersion using a local measurement, J. Phys. D: Appl. Phys. **44**, 464010 (2011).

[30] C. Gutiérrez, C.-J. Kim, L. Brown, T. Schiros, D. Nordlung, E. B. Lochoki, K. M. Shen, J. Park, and A. N. Pasupathy, Imaging chiral symmetry breaking from Kekulé bond order in graphene, Nat. Phys. **12**, 950 (2016).